Charles University in Prague
Faculty of Mathematics and Physics

DIPLOMA THESIS

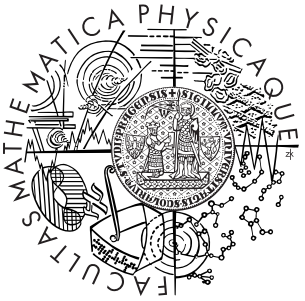

Jozef Sabo

Image de-blurring using two images with different exposure times

Department of Software and Computer Science Education

Supervisor: Ing. Filip Šroubek, Ph.D.
Study Program: Computer Science, Software Systems

2011

The author would like to thank the thesis supervisor, *Ing. Filip Šroubek, PhD.*, for his patience, goodwill and advice provided to him while writing this thesis and his family and friends for continued support.

I declare that I wrote the thesis by myself and listed all used sources. I agree to make the thesis publicly available.

Prague, December 9, 2011 Jozef Sabo

Contents

List of Figures

List of Tables

Název práce: Odstranění rozmazání pomocí dvou snímků s různou délkou expozice
Autor: Jozef Sabo
Katedra (ústav): Kabinet software a výuky informatiky
Vedoucí diplomové práce: Ing. Filip Šroubek, Ph.D.
e-mail vedoucího: sroubekf@utia.cas.cz

Abstrakt: V předložené práci studujeme metody odstranění rozmazání pomocí dvou snímků stejné předlohy s různou dobou expozicie, přičemž se soustřeďujeme na dvě hlavní kategorie těchto metod, tzv. dekonvoluční a nedekonvoluční. U obou kategorií rozebíráme jejich teoretické základy a zkoumáme jejich výhody a omezení. Samostatnou kapitolu věnujeme vyhodnocení a srovnání kategorií metod na testovacích datech (obrázky), k testování používáme metody implementovány v jazyku MATLAB. Účinnost zkoumaných metod srovnáváme i s vybraným odšumovacím algoritmem pracujícím s jedním vstupním obrázkem. Nesoustředíme se na výpočetní složitost srovnávaných algoritmů a pracujeme pouze se šedotónovými obrázky.

Klíčová slova: krátká a dlouhá, expozice, odstranění rozmazání, šum, odšumení, dekonvoluce

Title: Image de-blurring using two images with different exposure times
Author: Jozef Sabo
Department: Department of Software and Computer Science Education
Supervisor: Ing. Filip Šroubek, Ph.D.
Supervisor's e-mail address: sroubekf@utia.cas.cz

Abstract: In the presented work we study the methods of image de-blurring using two images of the same scene with different exposure times, focusing on two main approach categories, so called deconvolution and non-deconvolution methods. We present theoretical backgrounds on both categories and evaluate their limitations and advantages. We dedicate one section to a comparison both method categories on test data (images) for which we our MATLAB implementation of the methods. We also compare the effectiveness of said methods against the results of a selected single-image de-noising algorithm. We do not focus at computational efficiency of algorithms and work with grayscale images only.

Keywords: long and short, exposure, image de-blurring, noise, denoising, deconvolution

Chapter 1

Introduction

Image restoration[1] techniques have always been a subject of great interest within the domain of digital image processing. Their significance increases as digital photography undergoes rapid development with many digital imaging devices becoming readily available in countless forms, such as cell-phones, cameras and video cameras, to name a few.

We know from experience that it is quite difficult to obtain a quality image especially in insufficient lighting conditions requiring longer exposure times. In other words, taking "bad images" is easy. One of the most prevalent image degrading factors in photography is *motion blur*, caused either by motion in the photographed scene, the camera itself, or both. Suppression or complete removal of motion blur is highly desirable especially in hand-held devices.

According to [1], there are essentially two categories of approaches to deal with motion blur, the so-called *in-process* and *post-process*. The former focus at improving the conditions at which the image is being taken, usually by hardware means (e.g. image stabilizers), while the latter aim to correct the effects of motion blur after the image was taken. Widespread deployment of in-process-capable devices is however limited due to their high prices and as a result, the need for effective *post-process* algorithms arises.

In image processing, motion blur is modeled by discrete convolution. If a convolution operator (usually called *point-spread function* or *PSF*, sometimes more simply *kernel*) of motion blur is known (this applies to camera motion as local blurring caused by movement of objects in the scene tend to lead to *PSF* that is location-dependent - which is beyond the scope of this paper; however, some of

[1] Image restoration aims to reconstruct the original pre-degradation image as faithfully as possible as opposed to image enhancement, which aims to make desired features more visible. Contrast ehnancement, sharpening etc. are examples of image enhancement operations.

the methods to be mentioned below are capable of handling space-variant blurring naturally) the original image can be recovered by a deconvolution algorithm, such as Lucy-Richardson [2]. In most cases, there is little or no prior information on blur PSF which requires us to employ a *blind deconvolution* algorithm. First, a PSF is estimated from a given image or a set of images and subsequently, an existing *non-blind deconvolution* algorithm is used.

Blind deconvolution from a single image is a highly ill-posed problem that lacks a general solution. Blind deconvolution from multiple images (*multichannel blind deconvolution*) of the same scene subject to varying degrees of degradation (blur, noise), is better posed and leads to better results. The subject of this thesis is a special case of the multichannel blind deconvolution problem where we obtain two images of the same scene using different exposure times. The first image is taken using a long exposure time resulting in proper level of lighting but degraded by motion blur caused by camera shake, whereas the second image is taken using a short exposure time and is not affected by motion blur, but may be darker. Both images are affected by noise (the short exposure image is more noisy), which is dependent on the *ISO* sensitivity setting of the digital camera; we elaborate on this in greater detail in section 2.4.

There are several approaches how to restore the original image from the short and long exposure image pairs. These broadly fall in two categories – the *non-deconvolution* and *deconvolution* methods. The former do not perform deconvolution at any stage and try to utilize the image information in other ways as opposed to the latter, where deconvolution is performed at some point. Both categories feature methods with varying complexity, computational cost and efficiency, some of which will be described below. Section 2.3 elaborates on the problem of deconvolution.

The aim of this thesis is to analyze selected methods and evaluate their degree of suitability in various circumstances in terms of exposure times, signal-to-noise ratio improvements and other indicators based on experimental results. Methods are compared against themselves and we also compare them with a chosen single-image denoising algorithm to evaluate the benefits of additional image information in the form of improved quality of the restored image. We do not attempt to implement computationally effective algorithms at all costs nor do we provide an exhaustive list of all available methods. We perform experiments on both real-world and simulated data but focus on the latter, which allow the best degree of control over the experiment. Images are assumed to be grayscale[2] and registered. In case of real-world data, images are registered manually, if needed.

[2]Methods can be extended to process color images simply by applying them to each color channel separately. This is, however, not the subject of this thesis.

1.1 Structure of the text

TODO

Chapter 2

Research

This chapter provides .... basic background, what... TODO!

2.1 Model

For the purpose of de-blurring algorithms listed in the following chapters, we present a mathematical model of the short and long exposure image pair as mentioned above. Let $f(\mathbf{x})$ be the image function of the original, discrete, non-degraded grayscale image N^2 pixels in size. Let $g_2(\mathbf{x})$ be the image function of the original image subject to blurring and additive noise and finally let $g_1(\mathbf{x})$ be the image function of the underexposed image subject to additive noise only. According to Tico [4] we have:

$$\begin{aligned} \alpha g_1(\mathbf{x}) &= f(\mathbf{x}) &&+ n_1(\mathbf{x}) \\ g_2(\mathbf{x}) &= f(\mathbf{x}) \star d(\mathbf{x}) &&+ n_2(\mathbf{x}) \end{aligned} \tag{2.1}$$

where $\mathbf{x} = (x, y)$ are pixel coordinates, $d(\mathbf{x})$ is the point-spread function describing motion blur, α is the change in brightness as a result of shorter exposure (clearly $\alpha \leq 1$), $\star$ denotes the convolution operation and n_1, n_2 are noise terms. We assume additive Gaussian noise with $\mu_1 = \mu_2 = 0$ and $\sigma_1^2 \gg \sigma_2^2$ (where μ_i and σ_i^2 are the mean and variance respectively). We assume that g_1 is not blurred; however, the multichannel blind deconvolution method by Šroubek and Flusser (see section 2.8) and our extension can also handle blurring in the noisy image.

It is important to note that the assumption of zero-mean Gaussian noise is only used for the de-blurring process. Experimental data are generated in accordance with Foi's [3] noise model and Petteri M. Ojala's measurements [15]. These assumptions simplify theoretical derivation of de-blurring alghorithms; however,

they do not significantly affect their efficiency, as is shown in experimental results.

2.2 Blurred-noisy image pair problem

There are several methods to solve the blurred-noisy image pair problem, that is, using the notation from 2.1 to find an estimate $\hat{f}$ of the original image f such that $||\hat{f} - f||_2$ is minimized.

1. Enhance the short-exposure (noisy) image g_1 by removing noise, not considering the long-exposure (blurred) image g_2 at all. The BM3D denoising algorithm [19], used as a reference, fits into this category.

2. Enhance the short-exposure (noisy) image g_1 by using image statistics (standard deviation, mean) of the long-exposure (blurred) image g_2. This is the approach taken by Reinhard et al. [14]. A similar approach, aimed at enhancing image brightness and contrast by successive applications of 2 specialized functions is used by Razligh and Kehtarnavaz [5]. Since noise is present and is amplified by both methods, noise removal is necessary.

3. Regardless of α, perform blind deconvolution of the long-exposure (blurred) image g_2 making use of the image information present in short-exposure image g_1. Attempting blind deconvolution using only image g_2 is an underdetermined problem yielding unsatisfactory results. This is the approach taken by Lim and Silverstein [22], Tico in his 2006 and 2007 papers [4] [11], Babacan et al., [24], Yuan et al. [10] and others. The MCAM algoritm of Šroubek and Flusser [16], used in this thesis, is a multi-channel, multi-PSF generalization of the long-short exposure image pair problem, and is extended to accomodate different levels of noise in each channel. A more detailed description of the deconvolution problem is presented in section 2.3, Šroubek and Flusser's MCAM algorithm is presented in section 2.8.

4. Fuse images g_1 and g_2 without using deconvolution. The wavelet-based image fusion by Tico [6], described in 2.7 and used in this thesis, is a fitting example. The primary advantage of this algorithm stems from its ihnerent independence on the type of blurring.

2.3 Deconvolution problem

Referring to our model in equation 2.1, we have the image g_2 corrupted by blurring and noise, which is expressed as

$$g_2(\mathbf{x}) = f(\mathbf{x}) \star d(\mathbf{x}) + \ n_2(\mathbf{x}) \tag{2.2}$$

Our task is to reverse the blurring (convolution) process, remove as much noise as possible and present the best possible estimate $\hat{f}$ of the original image f. Quality of the estimation is assessed both visually and quantitatively, the usual requirement being the minimazation of mean squared error between the estimate and the original image. In many cases we also need to recover the blur PSF $d(\mathbf{x})$.

Deconvolution is a fairly non-trivial task. The amount of prior information about degradation, i.e., the size or shape of blurs, and the noise level, determines how mathematically ill-posed the problem is. Even non-blind restoration, when blurs are available, is in general an ill-posed problem because of zeros in the frequency domain of the blurs [16]. Without any prior knowledge of the blur PSF $d(\mathbf{x})$, we employ a *blind deconvolution* algorithm, which either provides the estimate in a single pass, or iteratively. The algorithm, based on assumptions that can be made, first estimates the blur PSF and then proceeds to remove the blur using a known, *non-blind* deconvolution algorithm.

One of the first deconvolution techniques was the *Wiener filter*. First, it can be used to estimate

The deconvolution process can significantly benefit from the presence of noisy image g_1, as it improves initial estimate of both $\hat{f}$ and $\hat{d}$.

2.4 Image noise in photography

In conventional photography, the photographic material's sensitivity to light is determined by the size of silver halide grains embedded in its emulsion. The larger a grain is, the more photons can it capture increasing the probability of exposure. Upon illumination, grains develop in an all-or-nothing fashion meaning that a grain decomposes into silver completely or not at all. This produces the characteristic "film grain" that is especially present in highly sensitive material used to shoot fast-moving scenes with very short shutter times.

Several systems were used to designate film sensitivity in the past. Among the most common were ASA, DIN and GOST. The ASA and DIN scales were incorporated into the new ISO standard published in 1987 (ISO 5800:1987) as the

ISO arithmetic scale and logarithmic scale, respectively. The ISO logarithmic scale gradually fell out of use in favor of the ISO arithmetic scale.

The process of capturing an image in a digital camera is somewhat different. Photographic material is replaced by an electronic image sensor which consists of an array of individual cells capable of converting light into electrical signals. This signal is then amplified, digitized and stored. Known types of image sensors include the CCD (*charge-coupled devices*) or CMOS (*complementary metal-oxide semiconductors*). CCD cells store captured light as an electrical charge until they are read (one at a time) whereas circuitry attached to each CMOS cell converts light energy into voltage directly. Neither technology has a clear advantage; CMOS sensors are however cheaper to manufacture.

Digital cameras typically allow the user to select from several ISO settings. This is made possible by varying the amplification factor affecting the signal leaving the image sensor. Since no image sensor is completely free of noise, amplification of the signal also amplifies noise, resulting in a lowered signal-to-noise ratio. Foi in [3] demonstrated that it is possible to model digital camera noise as two independent Gaussian (accounting for electrical and thermal noise) and Poissonian (accounting for the photon capturing process) components as follows:

$$g(\mathbf{x}) = f(\mathbf{x}) + \eta_p(f(\mathbf{x})) + \eta_g(\mathbf{x}) \tag{2.3}$$

where $\mathbf{x}$ is the pixel coordinate, $f(\mathbf{x})$ is the original image, $g(\mathbf{x})$ is the observed image and η_p and η_g are Poissonian and Gaussian noise components, respectively. In terms of distributions, the equation becomes

$$\begin{aligned} \chi(f(\mathbf{x}) + \eta_p(f(\mathbf{x}))) &\sim P(\chi f(\mathbf{x})) \\ \eta_g(\mathbf{x}) &\sim N(0, b) \end{aligned} \tag{2.4}$$

here $\chi \geq 0$ and $b \geq 0$ are real scalar parameters and N and P denote normal (i.e. Gaussian) and Poissonian distributions, respectively. Using $E\{\}$ for the expected value and $var\{\}$ for the variance of a random variable, we obtain

$$E\{\chi(f(\mathbf{x}) + \eta_p(f(\mathbf{x})))\} = var\{\chi(f(\mathbf{x}) + \eta_p(f(\mathbf{x})))\} = \chi f(\mathbf{x}) \tag{2.5}$$

from the properties of the Poisson distribution. Since

$$E\{\chi(f(\mathbf{x}) + \eta_p(f(\mathbf{x})))\} = \chi f(\mathbf{x}) + \chi E\{\eta_p(f(\mathbf{x}))\} \tag{2.6}$$

and

$$\chi^2 var\{\eta_p(f(\mathbf{x}))\} = \chi f(\mathbf{x}) \tag{2.7}$$

it follows that

$$E\{\eta_p(f(\mathbf{x}))\} = 0 \text{ and } var\{\eta_p(f(\mathbf{x}))\} = \frac{f(\mathbf{x})}{\chi} \tag{2.8}$$

The Poissonian η_p thus has variable variance that depends on the value of $f(\mathbf{x})$, $var\{\eta_p(f(x))\} = af(\mathbf{x})$ where $a = \chi^{-1}$. The Gaussian component η_g has constant variance equal to b. As a consequence, the total variance of the expression 2.3 can be expressed as

$$\sigma^2(f(\mathbf{x})) = af(\mathbf{x}) + b \tag{2.9}$$

Poissonian distribution can be approximated by normal distribution to a sufficient degree of accuracy by

$$P(\lambda) = N(\lambda, \lambda) \tag{2.10}$$

which combined with 2.8 and 2.9 yields

$$\eta_p(f(\mathbf{x})) + \eta_g(\mathbf{x}) \sim N(0, af(\mathbf{x}) + b) \tag{2.11}$$

The relationship between the ISO setting of a particular camera and parameters a and b are explored in [15] and adopted for use in this paper to generate experimental data.

2.5 Estimation of noise from images

The BM3D denoising algorithm, described in section 2.6, requires noise standard deviation σ as one of its input parameters. Hence, several methods to estimate σ from images are presented. Zero mean Gaussian noise is assumed in all cases. We present the methods in order of increasing complexity.

Immerkaer's method [20], published in 1996, is a simple and fast method that first smoothes the image using the Laplacian operator

$$N = \begin{pmatrix} 1 & -2 & 1 \\ -2 & 4 & -2 \\ 1 & -2 & 1 \end{pmatrix} \tag{2.12}$$

and follows with a direct estimation of the noise standard deviation σ using the formula

$$\sigma = \sqrt{\frac{\pi}{2}} \frac{1}{6(W-2)(H-2)} \sum_{\mathbf{x} \in I} |I(\mathbf{x}) \star N| \tag{2.13}$$

Altough the method is fast, its inherent simplicity causes it to perceive fine details (lines etc.) as noise, especially in highly textured images. An adaptive approach is therefore needed.

Tai and Yang's method [21], published in 1998, is an extension of the previous approach. First, the Sobel operator

$$\begin{aligned} G_x &= I(\mathbf{x}) \star \begin{pmatrix} -1 & -2 & -1 \\ 0 & 0 & 0 \\ 1 & 2 & 1 \end{pmatrix} \\ G_y &= I(\mathbf{x}) \star \begin{pmatrix} -1 & 0 & 1 \\ -2 & 0 & 2 \\ -1 & 0 & 1 \end{pmatrix} \\ G &= |G_x| + |G_y| \end{aligned} \tag{2.14}$$

is used to detect edges. In the following stage, it is necessary to estimate which regions are consired to be edges and therefore excluded from the computation of σ. This is achieved by thresholding G using threshold value G_{thr}, which is determined adaptively as a percentage $p\%$ of the image area that is to be considered as edge information. G_{thr} is set to a value where the cumulative histogram of G reaches $p\%$. This way, even if p is fixed, G_{thr} varies depending on the input image. After the exlusion of edge pixels, noise standard deviation is computed using Immerkaer's formula (2.13). Authors fix the p value at 10%.

Wavelet approach [7]. The wavelet approach to σ estimation uses the observation that wavelet transform distributes noise evenly across all scales, whereas image details are emphasized only at specific ones. First, the input image I is subject to discrete wavelet transform to obtain the first level, i.e. the finest detail coefficients $I_{1_{HVD}}$. The detail, horizontal and vertical transform coeffients are then grouped together to form a single array C_{HVD}. Median absolute deviation

$$\sigma = median_i(|C_{HVD}(i) - median_j(C_{HVD}(j))|) \tag{2.15}$$

is then used to yield the σ estimate[3].

An evaluation of the efficiency of these methods can be found in appendix D.

2.6 BM3D denoising algorithm

The BM3D denoising algorithm, short for block matching and 3D filtering, is a novel, highly efficient algorithm for still image denoising, introduced in 2006 by Alessandro Foi et al. in [19]. It is used in this thesis as a reference to verify the efficiency of the blurred-noisy image fusion.

[3] In other words, a median of a set of values is calculated first. Then, the median value is subtracted from each value in the set. The absolute value of each subtraction in the set is calculated and finally, median of the absolute values is computed yielding the median absolute deviation.

Historically, still image denoising algorithms predominantly work by attenuating noise in a suitable transform domain (FFT or wavelet transformation are amongst the most used). Altough transform-based methods are generally effective, they share common disadvantages such as introduction of unwanted artifacts and loss of detail often characteristic of a given approach.

The BM3D algorithm computes pixel values of the original image from image regions similar to the region centered at the estimated pixel. This approach introduces very few artifacts and, to prevent oversmoothing the image, regions are weighed adaptively. The image is processed pixel-by-pixel by means of a sliding window, regions similar to the currently processed window are stacked to form 3D arrays, inducing a high corellation between regions. A 3D decorrelating unitary transform τ_{3D} (such as DFT or DCT) which produces a sparse representation of the true signal in 3D transform domain is then performed, followed by efficient noise attenuation which is done by applying a shrinkage operator (e.g. hard-thresholding or Wiener filtering) on the transform coefficients. Blocks are then are reconstructed by an inverse 3D transform of the filtered coefficients. The final estimate is the weighted average of all overlapping local block-estimates. Because of overcompleteness which is due to the overlaping, blocking artifacts are avoided and estimation ability is further improved.

Since the BM3D algorithm is not the focus of this thesis and has only been reused, we present a brief description of the algorithm; more details can be found in [19]. It is important to note that the algorithm assumes noise standard deviation σ to be known a-priori, section 2.5 elaborates on methods of estimating it from images.

1. *Block matching.* For each pixel x and its corresponding block Z_x of size $N \times N$ (the pixel being located in the upper left block corner), a set S_x of similar image blocks is found. Block similarity is inversely proportional to block distance, which in turn is directly proportional to the L^2 norm of the difference between thresholded transformation τ_{2D} coefficients of a pair of evaluated blocks.

2. *Denoising in the 3D transformation domain.* Each set of blocks matching the reference block Z_x is stacked into a 3D array $\mathbf{S}_x$ (ordered by increasing block distance), subject to 3D transformation τ_{3D}, thresholding and inverse transformation, yielding the estimated array $\hat{\mathbf{S}}_x$. A weight coefficient $w_{\hat{\mathbf{S}}_x}$ is assigned to each estimate $\hat{\mathbf{S}}_x$; it is inversely proportional to the number of nonzero coefficients after τ_{3D} transformation and thresholding.

3. *Estimate aggregation.* After all reference blocks Z_x have been processed and their estimated block sets $\hat{S}_x$ computed, the final estimate is computed as a weighted average of all local ones.

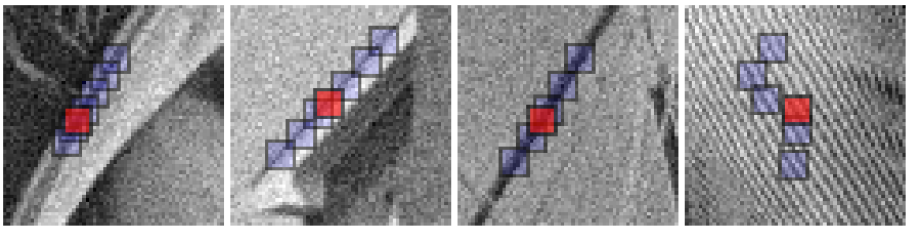

Figure 2.1: Cutaways of *Lena*, *House*, *Boats* and *Barbara* images corrupted by zero-mean additive Gaussian noise of $\sigma = 15/255$. A reference block R and a few of its matched ones illustrate block matching. Taken from [19].

2.7 Tico's wavelet method (2009)

Tico presents in [6] a relatively simple wavelet-based approach to blurred and noisy image fusion. Input images are first decomposed into their respective wavelet coefficients by using *undecimated* (also known as *stationary*) discrete wavelet transformation. Then, multi-level coefficient blending is performed. Finally, inverse wavelet transform is performed yielding the result image.

We observe that the absolute difference between the blurred and noisy images is due to presence of noise in the short-exposed image and blurring in the other. We therefore aim for an estimator that emphasizes the short-exposed image where the absolute difference between the two images is larger, and the long-exposed image otherwise. To achieve better separation between the signal and noise, an image estimator is derived in the wavelet domain. The edge locations (i.e., large values in the difference signal), are emphasized at some scales whereas the noise variance is evenly distributed across the scale space. Considering an orthonormal wavelet transform of the two images, denoting by $G_i(k)$, the k-th wavelet coefficient and assuming the same overall brightness of both images, we have

$$\begin{aligned} G_1(k) &= F(k) \quad + N_1(k) \\ G_2(k) &= F_b(k) \quad + N_2(k) \end{aligned} \tag{2.16}$$

Where F_b denotes the blurred image as a whole since the nature of blurring is not important in this case. Using the observation $\sigma_1^2 \gg \sigma_2^2$ we neglect the noisy coefficients $N_1(k)$ and the term $N_2(k)$ becomes $N(k)$.

We can now fuse the images together using different weights at different scales. Taking advantage of the de-correlation in the wavelet domain, we propose a minimum mean square error diagonal estimator of the original image in the

form of a linear combination between the wavelet coefficients of the two images

$$\widehat{F}(k) = G_1(k) + W(k)D(k) \tag{2.17}$$

where $\widehat{F}(k)$ stands for the wavelet coefficients of the restored image, $D(k) = G_2(k) - G_1(k)$ denotes the difference signal between the wavelet coefficients of the two observed images, and $W(k)$ are weight coefficients. We can estimate the best weight $W(k)$ for each wavelet coefficient by minimizing the mean squared error

$$E[\|\widehat{F}(k) - F(k)\|]_2^2 = E[\|G_1(k) - F(k) + W(k)D(k)\|]_2^2 \tag{2.18}$$

whose derivative with respect to $W(k)$ equated with zero yields

$$W(k)E[\|D(k)\|^2] = E[D(k)N(k)] \tag{2.19}$$

The computation of the weight $W(k)$ requires an estimate of the noise variance in the short-exposed image, and an estimate of the term $E[\|D(k)\|^2]$. In order to estimate noise variance in the short-exposed image the approach presented by Mallat in [7] where noise variance is calculated by using the median absolute deviation M_x [1] of the finest-scale wavelet coefficients as $\sigma \approx M_x/0.6745$ is used. Given the fact that in practice noise is spatially variant over the image, we apply the wavelet-based noise estimate in the pixel neighborhood (e.g. $7x7$). Finally, the $E[\|D(k)\|^2]$ is approximated with $max(\sigma^2(k), avg(|D(k)|^2))$ where avg denotes local spatial average and $\sigma^2(k)$ is the noise variance at the spatial location that corresponds to the k-th wavelet coefficient.

As a consequence, the weight $W(k)$ emphasizes the short exposed image in areas of image transitions (edges, for example) whereas the blurred image is emphasized in smooth regions.

2.8 Šroubek and Flusser's method (2003)

Šroubek and Flusser's MCAM algorithm, published in 2003 [16], presents a solution to the SIMO (*single input, multiple output*) multichannel blind deconvolution in the presence of noise, which is assumed to be Gaussian of zero mean and variance σ^2. We extend this algorithm to accomodate noise of different variance per each channel and use it in our 2 channel setting. It has been selected due to its high resilience to noise, no assumptions on the input PSFs and its potential to better accomodate real-life situations, as some amount of blurring typically occurs even in the short-exposed image.

[1] Median absolute deviation on an univariate sample of quantitative data is defined as $MAD = median_i(|X_i - median_j(X_j)|)$

Expressed mathematically, the algorithm assumes the input to be in the form

$$g_i(\mathbf{x}) = f(\mathbf{x}) \star d_i(\mathbf{x}) + n(\mathbf{x}) \tag{2.20}$$

where g_i are observed images, f is the original image, d_i are blur PSFs, n is Gaussian zero-mean noise of variance σ^2, $i \in \{1 \dots P\}$ is the channel number and $P \subset \mathbb{N}$ is the number of channels. As we can see, this approach is an extension of our model given by formula 2.1, albeit with the assumption of constant noise in each channel.

To achieve its task, the algorithm seeks to minimize the energy functional

$$E(f, d_1, \dots, d_P) = \frac{1}{2} \sum_{p=1}^{P} ||g_p - f \star d_p||^2 + \lambda Q(f) + \gamma R(d_1, \dots, d_P) \tag{2.21}$$

with respect to f and $d_1 \dots d_P$. $Q(f)$ and $R(d_1, \dots, d_P)$ are regularization terms for the original image and blur PSF estimates and λ and γ are parameters affecting their influence.

The regularization term $Q(f)$ adopts the total-variation form introduced by Rudin et al. in [23]

$$Q_{TV}(f) = \int_{\Omega} |\nabla f| \tag{2.22}$$

which, compared to other forms of regularization such as Tichonov's $Q_{TV}(f) = \int_{\Omega} |\nabla f|^2$ that assume f to be smooth and introduce unwanted ringing artifacts, provides better results. The regularization term $R(d_1, \dots, d_P)$ takes the form

$$R(d_1, \dots, d_P) = \sum_{1 \leq i < j \leq P} ||g_i \star d_j - g_j \star d_i||^2 \tag{2.23}$$

Making use of the vector-matrix notation, the P-channel acquisition model can be expressed as

$$\mathbf{g} = \mathcal{D}\mathbf{f} + \mathbf{n} = \mathcal{F}\mathbf{d} + \mathbf{n} \tag{2.24}$$

where $\mathbf{f} = [\mathbf{f_1}^T, \dots, \mathbf{f_P}^T]^T$ and $\mathbf{d} = [\mathbf{d_1}^T, \dots, \mathbf{d_P}^T]^T$ are aggregate vector forms of f and d. The matrices $\mathcal{D}$ and $\mathcal{F}$ are defined as

$$\mathcal{F} \equiv \begin{pmatrix} \mathbf{F} & \cdots & 0 \\ \vdots & \ddots & \vdots \\ 0 & \cdots & \mathbf{F} \end{pmatrix} \text{ and } \mathcal{D} \equiv \begin{pmatrix} \mathbf{D_1} \\ \vdots \\ \mathbf{D_P} \end{pmatrix} \tag{2.25}$$

where $\mathbf{F}$ and $\mathbf{D_i}$ are vector-matrix forms of f and d_i. The modified energy functional then assumes the form

$$E(\mathbf{d}, \mathbf{f}) = \frac{1}{2}||\mathcal{D}\mathbf{f} - \mathbf{g}||^2 + \lambda \mathbf{f}^T \mathcal{L} \mathbf{f} + \gamma ||\mathcal{Z}\mathbf{d}||^2 \tag{2.26}$$

Here, the use of $\mathcal{L}$ matrix achieves the computation of total variance from equation 2.22 in discrete form. The matrix $\mathcal{Z}$ achieves the same goal for the computation of regularization term in equation 2.23. Expanding the terms $\frac{1}{2}||\mathcal{D}\mathbf{f}-\mathbf{g}||^2$ (which is equivalent to $\frac{1}{2}||\mathcal{F}\mathbf{d}-\mathbf{g}||^2$) and $||\mathcal{Z}\mathbf{d}||^2$ yields the energy functional in the form

$$E(\mathbf{d},\mathbf{f}) = \frac{1}{2}[\mathbf{d}^T\mathcal{F}^T\mathcal{F}\mathbf{d} - 2\mathbf{g}^T\mathcal{F}\mathbf{d} + \mathbf{g}^T\mathbf{g}] + \lambda\mathbf{f}^T\mathcal{L}\mathbf{f} + \gamma\mathbf{d}^T\mathcal{Z}^T\mathcal{Z}\mathbf{d} \tag{2.27}$$

To obtain solutions for the minimal $\mathbf{d}$ and $\mathbf{f}$, we solve the system of differential equations

$$\begin{aligned} \frac{\partial E(\mathbf{d},\mathbf{f})}{\partial \mathbf{d}} &= 2\mathcal{F}^T\mathcal{F}\mathbf{d} \;\; - 2\mathcal{F}^T\mathbf{g} + 2\gamma\mathcal{Z}^T\mathcal{Z}\mathbf{d} \;\; = 0 \\ \frac{\partial E(\mathbf{d},\mathbf{f})}{\partial \mathbf{f}} &= 2\mathcal{D}^T\mathcal{D}\mathbf{f} \;\; - 2\mathcal{D}^T\mathbf{g} + 2\lambda\mathcal{L}\mathbf{f} \;\; = 0 \end{aligned} \tag{2.28}$$

from which we obtain the expressions for the solutions of $\mathbf{d}$ and $\mathbf{f}$

$$\begin{aligned} (\mathcal{F}^T\mathcal{F} \;\; + \gamma\mathcal{Z}^T\mathcal{Z})\mathbf{d} &= \mathcal{F}^T\mathbf{g} \\ (\mathcal{D}^T\mathcal{D} \;\; + \lambda\mathcal{L})\mathbf{f} &= \mathcal{D}^T\mathbf{g} \end{aligned} \tag{2.29}$$

and finally we obtain the values of $\mathbf{f}$ and $\mathbf{d}$ through the alternating minimization algorithm, which consists of the following steps.

Require: Initial value $\mathbf{f}^0$, blur size (m_d, n_d) and regularization parameters γ, λ

for $n \geq 1$ **do**
  $\mathbf{d}^n \leftarrow$ solve $[(\mathcal{F}^{n-1})^T\mathcal{F}^{n-1} + \gamma\mathcal{Z}^T\mathcal{Z}]\mathbf{d}^n = (\mathcal{F}^{n-1})^T\mathbf{g}$
  set $\mathbf{h}^0 = \mathbf{f}^{n-1}$ and $v^0 = \phi(\mathbf{f}^{n-1})$
  for $k \geq 1$ **do**
    $\mathbf{f}^k \leftarrow$ solve $[(\mathcal{D}^n)^T\mathcal{D}^n + \lambda\mathcal{L}v^{k-1}]\mathbf{f}^k = (\mathcal{D}^n)^T\mathbf{g}$
    $v^k = \phi(\mathbf{h}^k)$
  end for
  $\mathbf{f}^n \leftarrow \mathbf{h}^k$
end for

Parameters γ and λ providing the best results are usually obtained empirically, but can be estimated from equation 2.29 to obtain better starting values. Under the $\mathbb{L}_2$ norm, we obtain

$$\begin{aligned} \gamma^2 &= \frac{||\mathcal{F}^{\mathcal{T}}(\mathcal{F}\mathbf{d}-\mathbf{g})||^2}{||\mathcal{Z}^T\mathcal{Z}\mathbf{d}||^2} \\ \lambda^2 &= \frac{||\mathcal{D}^{\mathcal{T}}(\mathcal{D}\mathbf{f}-\mathbf{g})||^2}{||\mathcal{L}\mathbf{f}||^2} \end{aligned} \tag{2.30}$$

Since $F\mathbf{d}-\mathbf{g} = D\mathbf{f}-\mathbf{g}$ is equal to white Gaussian noise $\mathbf{n}$ and $||\mathbf{n}||^2 \approx Pm_fn_f\sigma^2$, it is easy to observe from the properties of vector-matrix notation that $||\mathcal{F}^T(\mathcal{F}\mathbf{d}-$

$\mathbf{g})||^2 \approx Pm_d n_d||\mathbf{f}||^2\sigma^2$. Given the fact that $\mathbf{d}$ stands for the correct PSFs, it must be a linear combination of $\mathcal{Z}^T\mathcal{Z}$ eigenvectors that correspond to a set of minimal eigenvalues, which can be expressed as $||\mathcal{Z}^T\mathcal{Z}\mathbf{d}||^2 = \lambda_1^2||\mathbf{d}||^2$. From the definition of $\mathcal{Z}$ it follows that $\lambda_1 \approx \sigma^2(P-1)m_f n_f$, yielding the final form of approximation

$$|\gamma| = \frac{1}{P-1}\frac{\sqrt{Pm_d n_d}}{||\mathbf{d}||}\frac{||\mathbf{f}||}{m_f n_f}\frac{1}{\sigma} \tag{2.31}$$

The $\mathbb{L}^2$ norms of $\mathbf{f}$ and $\mathbf{d}$ are not known in advance, but the former can be approximated by $\mathbf{g}$ and the latter, given that elements in each PSF must sum up to 1, is bound within $(P/(m_d n_d)^2) \leq ||\mathbf{d}||^2 \leq 1$.

A similar procedure is applied to the estimate of the λ parameter, but only a bottom limit can be obtained. The uncertainty resides in the term $||\mathcal{L}\mathbf{f}||^2$ which cannot be further simplified since it is completely dependent on the local behavior of f. The bottom limit in general is zero; the upper limit can be generously defined as $||\mathcal{L}\mathbf{f}||^2 \leq c^2||\mathbf{f}||^2$. The c constant is dependent on the used regularization term, that is $c = 4$ for the $\mathcal{L}_4$ and $c = 4 + 4(1/\sqrt{2})$ for the $\mathcal{L}_8$ TV. Given the fact that $||\mathcal{D}^T(\mathcal{D}\mathbf{f} - \mathbf{g})||^2 \approx ||\mathbf{d}||^2\sigma^2 m_f n_f$, the bottom limit is expressed as

$$|\lambda| \gtrapprox \frac{||\mathbf{d}||\sigma}{c}\frac{\sqrt{m_f n_f}}{||\mathbf{f}||} \tag{2.32}$$

The product of the parameters

$$|\gamma||\lambda| \geq \frac{1}{c(P-1)}\sqrt{\frac{Pm_d n_d}{m_f n_f}} \tag{2.33}$$

only depends on the dimension of the problem and establishes a fixed relation between them.

2.8.1 Algorithm extension

We propose and implement an extension to the MC-AM algorithm to allow for variable amount of noise in each channel. We assume each channel $i \in 1 \dots P$ to be corrupted by zero mean white Gaussian noise of variance σ_i^2, in other words

$$g_i(\mathbf{x}) = f(\mathbf{x}) \star d_i(\mathbf{x}) + n_i(\mathbf{x}) \tag{2.34}$$

To achieve this task, we need to balance the contribution of each channel to the overall minimization process. To this end, we need to analyze and assess the influence of variable noise on each of the terms in the energy fuctional described by equation 2.21 and modify it accordingly.

The first term

$$\sum_{p=1}^{P} ||g_p - f \star d_p||^2 \tag{2.35}$$

can be expanded as

$$\sum_{p=1}^{P} ||g_p - f \star d_p||^2 = ||n_1||^2 + ||n_2||^2 + \cdots + ||n_P||^2 \approx m_f n_f \sigma_1^2 + m_f n_f \sigma_2^2 + \cdots + m_f n_f \sigma_P^2 \tag{2.36}$$

from which we can directly observe that each term needs to be multiplied by σ_p^{-2} to balance its contribution, we thus obtain

$$\sum_{p=1}^{P} \frac{||g_p - f \star d_p||^2}{\sigma_p^2} \tag{2.37}$$

as the modification of the first term.

The second, total variation term will not be modified as it is a function of the original image f. Its initial value for the algorithm is provided by g_i as is the case in the unmodified version. It is however important to note that the value of the parameter λ will change as a result of our modification, as will be described below.

The third, blur PSF regularization term $R(d_1 \dots d_P)$ is a sum of terms $||g_i \star d_j - g_j \star d_i||^2$, where $1 \leq i < j \leq P$. It can be expanded as

$$\begin{aligned} ||g_i \star d_j - g_j \star d_i||^2 &= ||(f \star d_i + n_i) \star d_j - (f \star d_j + n_j) \star d_i||^2 \\ &= ||f \star d_i \star d_j - f \star d_j \star d_i + n_i \star d_j - n_j \star d_i||^2 \\ &= ||n_i \star d_j - n_j \star d_i||^2. \end{aligned} \tag{2.38}$$

The term $||n_i \star d_j - n_j \star d_i||^2$ can be simplified further. When we think of convolution, we can visualize it as α-blending of $m_d n_d$ shifted copies of the original image, where $\sum \alpha_i = 1$. Doing the same with noise results also in noise with approximately the same characteristics. We can therefore write

$$||n_i \star d_j - n_j \star d_i||^2 \approx ||n_i - n_j||^2 \tag{2.39}$$

Since terms n_i and n_j represent uncorrelated noise and $||\dots||^2 = (\dots)^T(\dots)$, we obtain

$$\begin{aligned} ||n_i - n_j||^2 &= (n_i - n_j)^T (n_i - n_j) \\ &= n_i^T n_i - n_j^T n_i - n_i^T n_j + n_j^T n_j \\ &= n_i^T n_i + n_j^T n_j \\ &\approx m_f n_f (\sigma_i^2 + \sigma_j^2). \end{aligned} \tag{2.40}$$

The regularization term $R(d_1 \dots d_P)$ thus assumes the form

$$R(d_1, \dots, d_P) = \sum_{1 \le i < j \le P} \frac{1}{\sigma_i^2 + \sigma_j^2} ||g_i \star d_j - g_j \star d_i||^2 \tag{2.41}$$

In discrete form, weights are introduced into the first term by matrix multiplication using a diagonal matrix Σ containing noise standard deviations σ_i

$$\left|\left| \begin{pmatrix} \sigma_1^{-1} & \dots & 0 \\ \vdots & \ddots & \vdots \\ 0 & \dots & \sigma_P^{-1} \end{pmatrix} \left[\begin{pmatrix} \mathbf{F} & \dots & 0 \\ \vdots & \ddots & \vdots \\ 0 & \dots & \mathbf{F} \end{pmatrix} \begin{pmatrix} \mathbf{d_1} \\ \dots \\ \mathbf{d_P} \end{pmatrix} - \begin{pmatrix} \mathbf{g_1} \\ \dots \\ \mathbf{g_P} \end{pmatrix} \right] \right|\right|^2 . \tag{2.42}$$

Rather than altering the matrix $\mathcal{Z}$ which is not used directly, we modify the matrix product $\mathcal{Z}^T\mathcal{Z}$ as follows

$$\mathcal{Z}^T\mathcal{Z} = (\mathcal{Z}_{ij}) = \begin{cases} \frac{1}{\sigma_i^2+\sigma_j^2}\mathbf{G}_j^T\mathbf{G}_i, & i \neq j \\ \sum_{k \neq i} \frac{1}{\sigma_i^2+\sigma_k^2}\mathbf{G}_k^T\mathbf{G}_k, & i = j \end{cases} \tag{2.43}$$

It is necessary to determine how our modification will affect the estimation of γ and λ parameters. We can easily observe that the introduction of the Σ weight matrix will modify the numerator in both γ^2 and λ^2 estimation (see equation 2.30) as $||\mathcal{F}^T\Sigma^T\Sigma(\mathcal{F}\mathbf{d} - \mathbf{g})||^2$ and $||\mathcal{D}^T\Sigma^T\Sigma(\mathcal{D}\mathbf{f} - \mathbf{g})||^2$, respectively. Since

$$||\mathcal{F}^T(\mathcal{F}\mathbf{d} - \mathbf{g})||^2 \approx P m_d n_d ||\mathbf{f}||^2 \sigma^2 \tag{2.44}$$

and

$$||\mathcal{D}^T(\mathcal{D}\mathbf{f} - \mathbf{g})||^2 \approx ||\mathbf{d}||^2 \sigma^2 m_f n_f \tag{2.45}$$

and σ_i^{-2} emerge from the $\mathbb{L}_2$ norm as σ_i^{-4}, we obtain the modified numerators in the form

$$||\mathcal{F}^T(\mathcal{F}\mathbf{d} - \mathbf{g})||^2 \approx m_d n_d ||\mathbf{f}||^2 \sum_{i=1}^{P} \frac{1}{\sigma_i^2} \tag{2.46}$$

and

$$||\mathcal{D}^T(\mathcal{D}\mathbf{f} - \mathbf{g})||^2 \approx m_f n_f \sum_{i=1}^{P} \frac{||\mathbf{d}_i||^2}{\sigma_i^2} \tag{2.47}$$

The denominator $||\mathcal{L}\mathbf{f}||^2$ in the λ^2 estimation equation remains unaffected. To evaluate the change in the $||\mathcal{Z}^T\mathcal{Z}\mathbf{d}||^2$ denominator, let us first assume that each of the P channels is corrupted by Gaussian zero-mean noise of the same variance σ^2. This will, according to our modification of the $\mathcal{Z}^T\mathcal{Z}$ matrix in equation 2.43, lead to a matrix in which each element is multiplied by $1/2\sigma^2$. Thus, in this special case, we obtain the modified $\mathcal{Z}^T\mathcal{Z}$ matrix simply by multiplying the original

by $1/2\sigma^2$. Given the above observation $||\mathcal{Z}^T\mathcal{Z}\mathbf{d}||^2 \approx (\sigma^2(P-1)m_f n_f)^2||\mathbf{d}||^2$; moreover,

$$\begin{aligned}\gamma^2 &= \frac{||\mathcal{F}^{\mathcal{T}}(\mathcal{F}\mathbf{d}-\mathbf{g})||^2}{||\mathcal{Z}^T\mathcal{Z}\mathbf{d}||^2} \\ \lambda^2 &= \frac{||\mathcal{D}^{\mathcal{T}}(\mathcal{D}\mathbf{f}-\mathbf{g})||^2}{||\mathcal{L}\mathbf{f}||^2}\end{aligned} \tag{2.48}$$

Chapter 3

Results

3.1 Experimental setup

3.1.1 Setup for simulated data

We have selected a set of 4 point spread functions (see figure 3.1) and 4 testing images (see figure 3.1). These were selected in order to reflect various environments and conditions in which taking images could take place.

Figure 3.1: Point-spread functions selected for use in testing

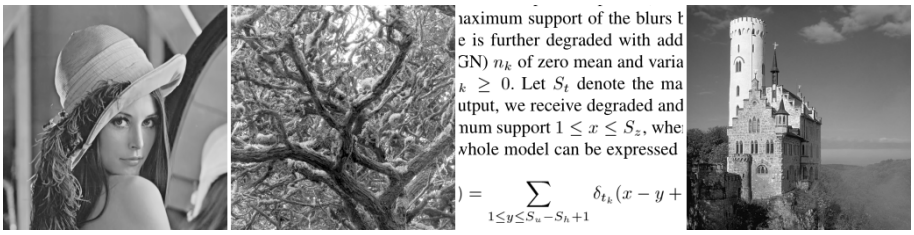

Figure 3.2: Images selected for use in testing

Testing images used were 256 by 256 pixels in size. We avoided the use of larger resolutions since they tend to be computationally expensive. PSF sizes were varied in the range of $2^n - 1$, with n being an integer in range $\{2 \dots 5\}$. Real-world experiments suggest the worst-case PSF size at about 1/100 of the original image. This is only a rough rule, since the ratio greatly depends on the individual photographer's steadiness while taking a picture.

Since Ojala in [15] demonstrated that temperature and exposure time have very little influence on the level of noise present in a digital photograph, we chose to abandon these parameters completely, leaving ISO as the only parameter. ISO 100 was chosen as the base value for both generated and real-world data.

In case of generated data, the pair of ISO values is not obtained empirically, but chosen in advance, one of the values being 100 for the blurred, less noisy image. The other value is set to $100 * 2^i$, where i is an integer greater than 1. This corresponds to ISO settings usually present in digital cameras; however, as of 2011, ISO settings over 12800 are rarely encountered in commercially available products, requiring us to use a value of i no greater than 7.

Fixing the low ISO value at 100, the choice of the high ISO value depends on the level of illumination we wish to emulate. The lower the amount of light, the higher ISO we need to compensate for the potentially longer exposure time (and thus larger blurring) needed for the camera to capture enough light.

3.1.2 Setup for real-world data

Real-world experiments were performed by projecting the Lena image on a vertical white wall 2.6 by 2.6 metres in size and taking images of it with a Canon EOS 5D digital SLR camera using an 85 mm lens at a distance of 5 meters. The projector's optical axis was not perpendicular to the projecting wall; however, a dedicated setting of the projector was used to compensate. The projected image was 70 by 70 centimeters in size and was carefully measured vertically, horizontally and diagonally to rule out any spatial distortion. Sources of light other than the projector itself were blocked out to prevent light pollution and color interference. Control over the level of illumination was achieved by multiplying the image function by a constant; 0.5, 0.25 and 0.125 were the values used (the resulting images were too bright for multiplier 1 - the original Lena image). Since the projector's output resolution was 800 by 600 pixels and the used image was 256 by 256 pixels in size, it was possible to insert control features (pixels and crosses) in the otherwise unused part of the projected space (see 3.4). These features were used to align the obtained images and to directly observe PSF shapes.

Figure 3.3: Setup for real-world testing

Three experiments were carried out, one for each multiplier value. In each experiment, several (about 20) images were taken at a progressively greater ISO setting until the images produced contained little or no blurring. All images were taken in aperture priority mode with aperture set to the lowest possible value, 1.8. For each experiment, a set of two images was selected; the first taken with ISO set to 100 (the "blurred" image) and the second taken at the lowest ISO setting that produced little or no blurring (the "noisy" images). These images were processed as follows:

1. Images are converted from 24 bits per pixel color JPEG to 8 bits per pixel PNG.

2. Images are semi-manually registered in Matlab using the `cpselect`, `cp2tform` and `imtransform` routines. The registration process (see figure 3.5) also downsamples the images from their original 4368 by 2912 pixels resolution to less than 800 by 600 needed for further processing.

3. Registered images are manually aligned (Paint.NET image editor was used). Figure 3.15 illustrates the result of one such alignment.

4. PSF size for the blurred image is determined by fitting the blur kernel in the smallest possible odd-sized square region with a small margin.

Figure 3.4: An example of a testing image with control features

5. Central region of size $m_u - m_d + 1$ by $n_u - n_d + 1$ is cut from the original, blurred and noisy image in their aligned position.

6. Blurred and noisy images obtained by cropping in the previous step have their statistics (mean and standard deviation) matched with the original Lena image using the color transfer method by Reinhard et al.[14]

7. Noise standard deviation is estimated from both images as an average value of the results of the 4 available methods (see section 2.5).

8. The noisy image is denoised by the BM3D algorithm using the estimated noise standard deviation value.

9. The noisy and blurred images are subject to Tico's wavelet fusion and Šroubek's MC-AM deconvolution.

10. Resulting images are evaluated.

Experiment 1, multiplier 0.125.

In this experiment, the blurred image was obtained using the ISO setting of 100 and 2.5 second exposure time. The noisy image was obtained with the ISO

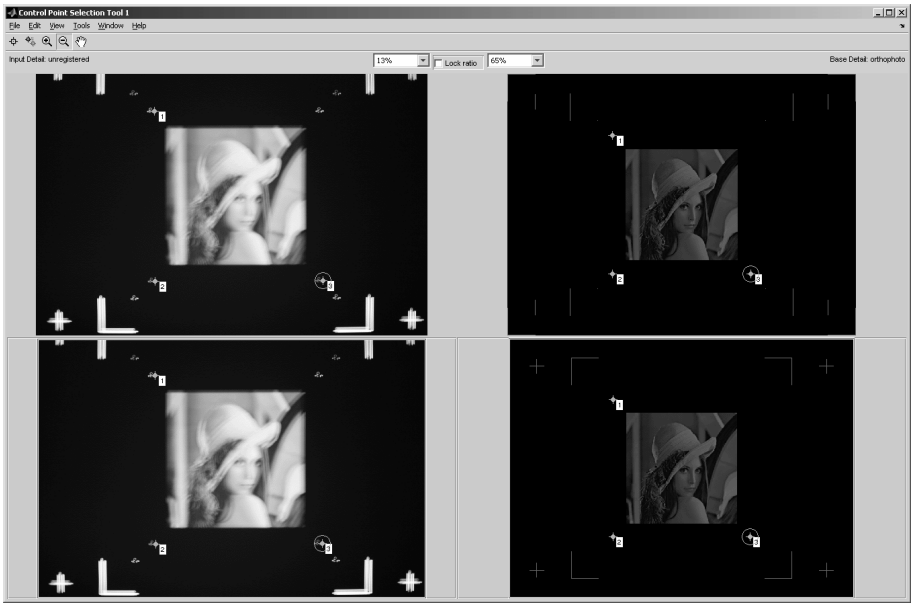

Figure 3.5: Image registration process in Matlab, feature point selection.

setting of 1600 and 1/6 second exposure time. The blurred image's blur kernel size was determined to be 31 by 31 pixels, blurring was also present in the noisy image with blur kernel size 9 by 9 pixels.

Experiment 2, multiplier 0.25

In this case, the blurred image was obtained using the ISO setting of 100 and 1 second exposure time. The noisy image was again obtained with the ISO setting of 1600 and 1/15 second exposure time. The blurred image's blur kernel size was determined to be 21 by 21 pixels, blurring in the noisy image was also present, at 5 by 5 pixels.

Experiment 3, multiplier 0.5

The blurred image was taken using the ISO setting of 100 and 1/3 second exposure time, resulting in a blur kernel 17 by 17 pixels in size. The noisy image, obtained with the ISO setting of 1000 and 1/30 was blurred by a kernel 5 by 5 pixels in size.

Figure 3.6: The result of image alignment for experiment 1.

3.2 Generated data

3.3 Real-world data

3.4 Evaluation

Figure 3.7: The original, blurred and noisy images for experiment 1.

Figure 3.8: The original, blurred and noisy images for experiment 1 with their statistics matched.

Figure 3.9: The result for Tico, Šroubek and BM3D methods for experiment 1.

Figure 3.10: The original, blurred and noisy images for experiment 2.

Figure 3.11: The original, blurred and noisy images for experiment 2 with their statistics matched.

Figure 3.12: The result of Tico, Šroubek and BM3D methods for experiment 2.

Figure 3.13: The original, blurred and noisy images for experiment 3.

Figure 3.14: The original, blurred and noisy images for experiment 3 with their statistics matched.

Figure 3.15: The result of Tico, Šroubek and BM3D methods for experiment 3.

Chapter 4

Conclusion

We have studied and described several methods of image deblurring using two images with different exposure times. We have established two categories, the *deconvolution* and *non-deconvolution* methods. We have selected one method from each category, tested them on generated as well as real-world data and compared them to each other and to the results of a state-of-the-art denoising algorithm (BM3D) performed on the noisy image (g_2 from 2.1, specifically). We have, given the experimental results, demonstrated that:

- In a majority of cases, using two images with different exposure times provides no additional benefit over single-image denoising
- Two-image deblurring algorithms "defeat" single image denoising in rare cases and in conditions too extreme to be attained by conventional photography
- In low-noise conditions, using a *non-deconvolution* method generally provides better results than using a *deconvolution* method
- All tested methods generally fail on data exhibiting self-similarity and other non-standard behavior rarely present in conventional photographs

This leads us to a general conclusion that an efficient single image denoising algorithm provides better results than using two images with different exposure times.

4.1 Possible future improvements

TODO

Appendix A

Evaluation methods

Given the estimate $\hat{f}$ of the original image f, several methods can be used to evaulate the quality of the estimation.

TODO Šroubek SNR

Appendix B

Implementation and testing notes

Methods tested in this paper have been implemented using Matlab version 7.3.0 running on Microsoft Windows XP Professional SP 2. Apart from standard Matlab functions, the *Wavelet Toobox* and *Image Processing Toolbox* were used.

Tests were performed on a single-core 1.8 GHz PC running 32-bit Microsoft Windows XP Professional SP 2 with 1792 MB of RAM.

No GUI was implemented and tests were performed in batch mode, results being written to a *.csv file. This is readable in plain text, but is better wieved in a spreadsheet processor, such as Microsoft Excel or Libre Office.

Appendix C

Ojala's ISO measurements

Appendix D

Efficiency of noise estimation methods

Bibliography

[1] Jia J., Sun J., Tang C.K., Shum H.Y.: *Bayesian correction of image intensity with spatial consideration*, Proceedings of the eighth European Conference on Computer Vision, 256-266, Praha, 2004

[2] Richardson, W. H.: *Bayesian-Based Iterative Method of Image Restoration*, JOSA, Volume 62, 2007

[3] Foi A., Trimeche M., Katkovnik V., Egiazarian K.: *Practical Poissonian-Gaussian noise modeling and fitting for single-image raw-data*, IEEE Transactions, 2007

[4] Tico M., Vehvilainen M.: *Estimation of motion blur point spread function from differently exposed images*, Nokia Research Center, Tampere, Finland, 2006

[5] Razligh Q.R., Kehtarnavaz N.: *Image blur reduction for cell-phone cameras via adaptive tonal correction*, Department of Electrical Engineering, University of Texas at Dallas, 2007

[6] Tico M., Pulli K.: *Image enhancement via blur and noisy image fusion*, Nokia Research Center, Palo Alto, CA, USA, 2009

[7] Mallat, S.: *A wavelet tour of signal processing, the sparse way*, Elsevier, Burlington, MA, 2009

[8] Rao, A.R.: *A Taxonomy for Texture Description and Identification*, Springer Verlag, 1990

[9] Liu X., Gamal A.: *Simultaneous image formation and motion blur restoration via multiple capture*, Proceedings of the International Conference on Acoustics, Speech, Signal Processing, 2001

[10] Yuan L., Sun J., Quan L., Shum H.Y.: *Image Deblurring with blurred/noisy image pairs*, Computer Science Department, Hong Kong University of Science and Technology, 2007

[11] Tico M., Vehvilainen M.: *Image stabilization based on fusing the visual information in differently exposed images*, Nokia Research Center, Tampere, Finland, 2007

[12] Beneš B., Felkel P., Sochor J., Žára J.: *Moderní počítačová grafika, 2. vydání*, Computer Press, 2004

[13] Biedl T., Chan T., Demaine E., Fleischer R., Golin M., King J., IanMun J.: *Fun Sort - or the Chaos of Unordered Binary Search*, Discrete Applied Mathematics, vol. 144, p. 231-236, 2004

[14] Gooch M., Reinhard E., Ashikmin E., Shirley P.: *Color transfer between images*, IEEE Computer Graphics and Applications, 34-40, 2001

[15] Petteri, O. M.: *Dependence of the parameters of digital image noise model on ISO number, temperature and shutter time*, Tampere University of Technology, Department of Automation Science and Engineering, Tampere, Finland, 2008

[16] Šroubek F., Flusser J.: *Multichannel Blind Iterative Image Restoration*, Proceedings of IEEE Transactions on Image Processing, vol. 12, No. 9, September 2003

[17] *The USC-SIPI Image Database*
`http://sipi.usc.edu/database/`

[18] *Wikipedia*, miscellaneous articles.
`http://en.wikipedia.org/`

[19] Dabov K., Foi A., Katkovnik V., Egiazarian K.: *Image denoising with block-matching and 3D filtering*, Institute of Signal Processing, Tampere University of Technology, PO BOX 553, 33101 Tampere, Finland, 2006

[20] Immerkær J.: *Fast noise variance estimation*, Computer Vision and Image Understanding, Vol. 64, No. 2, 300-302, 1996

[21] Tai S. Ch., Yang S. M.: *A fast method for image noise estimation using laplacian operator and adaptive edge detection*, Proceedings of the second International Symposium on Communications, Control and Signal Processing, 1077-1081, 2008.

[22] Lim S. H., Silverstein A.: *Estimation and removal of motion blur by capturing two images with different exposures*, Hewlett-Packard Laboratories, 2008.

[23] Rudin L., Osher S., Fatemi E.: *Nonlinear total variation based noise removal algorithms*, Phys. D, vol. 60, 259–268, 1992.

[24] Babacan S.D., Wang J., Molina R., Katsaggelos A.K.: *Bayesian blind deconvolution from differently exposed image pairs*, Proceedings of the 2009 IEEE International Conference on Image Processing, 133-136, 2009.